Journal of Systems Engineering and Electronics
Vol. 32, No. 4, August 2021, pp.789 – 798

Multi-objective robust secure beamforming for cognitive satellite and UAV networks

WANG Zining[1], LIN Min[1,*], TANG Xiaogang[2], GUO Kefeng[2], HUANG Shuo[3], and CHENG Ming[1]

1. School of Telecommunications and Information Engineering, Nanjing University of Posts and Telecommunications, Nanjing 210003, China; 2. School of Space Information, Space Engineering University, Beijing 101407, China; 3. Shanghai Aerospace Electronic Technology Institute, Shanghai 201109, China

Abstract: A multi-objective optimization based robust beamforming (BF) scheme is proposed to realize secure transmission in a cognitive satellite and unmanned aerial vehicle (UAV) network. Since the satellite network coexists with the UAV network, we first consider both achievable secrecy rate maximization and total transmit power minimization, and formulate a multi-objective optimization problem (MOOP) using the weighted Tchebycheff approach. Then, by supposing that only imperfect channel state information based on the angular information is available, we propose a method combining angular discretization with Taylor approximation to transform the non-convex objective function and constraints to the convex ones. Next, we adopt semi-definite programming together with randomization technology to solve the original MOOP and obtain the BF weight vector. Finally, simulation results illustrate that the Pareto optimal trade-off can be achieved, and the superiority of our proposed scheme is confirmed by comparing with the existing BF schemes.

Keywords: cognitive satellite and unmanned aerial vehicle network (CSUN), multi-objective optimization, robust secure beamforming (BF), weighted Tchebycheff approach.

DOI: 10.23919/JSEE.2021.000068

1. Introduction

Recently, application of satellite communication (SatCom) in future wireless systems has attracted significant attention, since it can provide ubiquitous connections and high quality service for users all over the world [1−4]. Meanwhile, compared with SatCom, unmanned aerial vehicles (UAVs) has the advantages of adjusting their altitudes conveniently and avoiding obstacles to establish line-of-sight (LoS) communication links, so that the quality of communication links can be improved efficiently. As such, UAV technology is developing rapidly, which has been widely used in many fields, such as surveillance and monitoring, and emergency communications [5−9].

To take advantages of both SatCom and UAV communications, the 3rd Generation Partnership Project (3GPP) has proposed to use both satellites and UAVs as integrated access platforms for the next generation wireless communications [10]. However, the scarcity of spectrum resources has become a bottleneck to further enhance the capacity of wireless systems. To address this issue, the concept of cognitive satellite and UAV networks (CSUNs) that utilizes the cognitive radio (CR) to realize the spectrum coexistence of both SatCom and UAV networks has been introduced in [11−13] and attracted increasing attention. Specifically, the authors of [11] investigated the multi-domain resource allocation to improve the efficiency of massive access for CSUNs. In [13], the authors proposed a cooperative beamforming (BF) scheme to achieve energy-efficient communication in CSUNs.

Besides realizing the spectrum coexistence in CSUNs, another urgent issue is the privacy and security, which is due to the broadcasting nature of wireless communications. In this regard, the cryptographic encryption method is commonly used at the upper layer to achieve secure transmission. However, this security scheme faces great challenges with the rapid development of computational capability, especially the application of quantum computing. By exploiting signal processing and the randomness of wireless channels, the physical layer security (PLS) is considered as a promising approach to achieve secure

Manuscript received February 01, 2021.
*Corresponding author.
This work was supported by the Key International Cooperation Research Project (61720106003), the National Natural Science Foundation of China (62001517), the Shanghai Aerospace Science and Technology Innovation Foundation (SAST2019-095), the NUPTSF (NY220111), and the Foundational Research Project of Complex Electronic System Simulation Laboratory (DXZT-JC-ZZ-2019-009; DXZT-JC-ZZ-2019-005).

communication. Since BF technology is capable of both enhancing the received signal at the legitimate users and suppressing the signal to eavesdroppers (Eves), the employment of BF in PLS to improve the secrecy performance of the system has become a new research hotspot [14−16]. For example, in [14], the authors proposed a BF method using semi-definite programming (SDP) combined with one-dimension search to maximize the sum secrecy rate in multibeam SatCom. Considering the scenarios of single Eve and multiple Eves, respectively, the authors of [15] proposed two joint BF schemes to improve the security of integrated satellite terrestrial networks. It is worth mentioning that the previous work in [14] and [15] has assumed that perfect channel state information (CSI) is available at the transmitter, which is unrealistic in some cases due to the estimation error, mobility of terminals and limited feedback channels [17]. Thereby, the authors of [18] proposed a robust BF scheme to maximize the secrecy rate for a two-tier heterogeneous cellular network, where the *S*-procedure is adopted to transform quadratic matrix inequality constraints into linear matrix inequality. In [19], the authors investigated the robust secure BF and power splitting for cognitive satellite and terrestrial networks (CSTNs).

Although the aforementioned works have conducted in-depth investigations on PLS in wireless communications, they only focused on the single performance criterion, such as the transmit power or the achievable secrecy rate (ASR). Actually, the next generation wireless network aims at providing a variety of services with high transmission rates, high reliability, low energy consumption and low latency. In this context, the multi-objective optimization problem (MOOP) implementing the trade-off between multiple objectives has attracted much interest in recent years [20−22]. In [20], the MOOP about the trade-off between the total transmit power and the energy harvesting efficiency was investigated for a multiuser multiple-input single-output downlink system. The authors of [21] investigated the MOOP through the modified weighted Tchebycheff approach. In [22], the authors adopted semidefinite programming relaxation to solve the MOOP about total downlink and uplink transmit power minimization. Besides, the MOOP for secure beamforming design of CSTNs was studied in [23], where the perfect CSI was used to conduct the optimization design. The most existing multi-objective research focuses on the system design in terrestrial networks or CSTNs, whereas the application of the multiple objective problem in CSUNs is still an open yet challenging topic that needs to be studied further.

Motivated by these observations, we propose a multi-objective optimization based robust BF scheme under the condition of imperfect CSI to achieve the trade-off between the ASR and the total transmit power in CSUNs. In summary, the contributions of this paper can be listed as follows:

(i) We present a framework to implement PLS in the CSUNs, where the satellite is equipped with array fed reflector antennas and the UAV employs uniform planar arrays (UPAs). With the help of CR technology, the satellite network termed as the primary network shares spectrum resources with the UAV network termed as the secondary network. In this context, it is urgent to investigate new BF schemes that should consider multiple objectives in wireless communications.

(ii) We adopt the weighted Tchebycheff approach to implement the trade-off between the ASR and the total transmit power, while the total transmit power budget and the quality-of-service requirements of secondary users (SUs) and primary users (PUs) are chosen as the constraints. Compared with the existing work in [18] and [19], which only takes single objective optimization into account, our proposed scheme can achieve the Pareto optimal trade-off between the multiple objectives [24].

(iii) Considering that only the imperfect CSI based on angular information of PUs and Eves is known, we propose a method combining angular discretization with Taylor approximation to transform the non-convex objective function and constraints to the convex ones and obtain the BF weight vector through SDP joint with a randomization technology. Compared with other existing methods, our proposed method can offer a global optimal solution with a fast convergence. We utilize the imperfect CSI to perform robust BF design, which is more realistic than BF schemes based on perfect CSI in previous works, such as [21] and [23].

The rest of this paper is organized as follows: Section 2 introduces the system model and formulates the MOOP. In Section 3, the robust BF scheme is proposed to solve the MOOP. Section 4 provides simulation results and discussions. Finally, we conclude our paper in Section 5.

2. System model and problem formulation

As shown in Fig. 1, we investigate the downlink transmission of a CSUN, where the satellite network acting as the primary network shares the spectrum resources with the UAV network termed as the secondary network. The geostationary orbit (GEO) satellite exploits multicast transmission to provide wireless services to L PUs, while the UAV transmits the private signal to an SU that will be wiretapped by K Eves within its coverage. The satellite employs array fed reflector antennas with N_s feeds and the UAV is equipped with a UPA having N_u antennas.

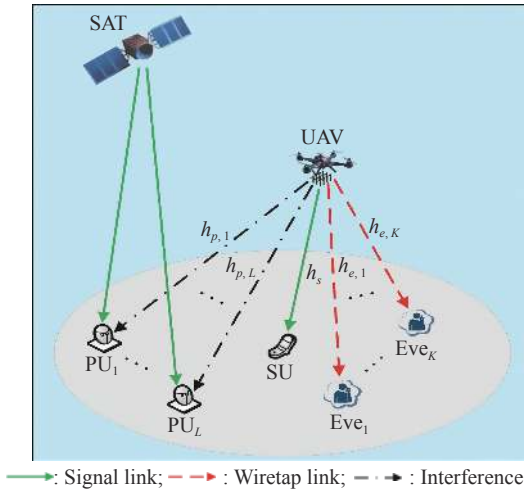

Fig. 1 System model

Similar to the related work [25], we assume that the interference from satellite to SU and Eves can be ignored owing to the large path loss of satellite links. The UAV performs transmit BF with weight vector $\boldsymbol{w} \in \mathbb{C}^{N_u \times 1}$ and transmits message $s(t)$ satisfying $\mathrm{E}[|s(t)|^2] = 1$ to the SU, where $\mathrm{E}[\cdot]$ represents the expectation, $\mathbb{C}^{N_u \times 1}$ denotes the complex space of $N_u \times 1$ and $|\cdot|$ represents the absolute value. After passing through the wireless channel, the received signals at the SU and the kth Eve can be, respectively, expressed as

$$y_s = \boldsymbol{h}_s^{\mathrm{H}} \boldsymbol{w} s(t) + n_s(t), \tag{1}$$

$$y_{e,k} = \boldsymbol{h}_{e,k}^{\mathrm{H}} \boldsymbol{w} s(t) + n_{e,k}(t), \forall k, \tag{2}$$

where $(\cdot)^{\mathrm{H}}$ denotes the Hermitian transpose, $\boldsymbol{h}_i (i \in \{s,(e,k)\})$ denotes the channel vector from UAV to the SU or the kth Eve. $n_s(t)$ and $n_{e,k}(t)$ denote independent and identically distributed (i.i.d) additive white Gaussian noise (AWGN) with zero mean and variances $\sigma_i^2 = \kappa B T (i \in \{s,(e,k)\})$, where T denotes the receive noise temperature, B is the noise bandwidth and $\kappa \approx 1.38 \times 10^{-23}$ J/K represents the Boltzmanns constant. According to (1) and (2), the output signal-to-noise ratio (SNR) at the SU and the kth Eve are, respectively, given by

$$\gamma_s = \frac{\left|\boldsymbol{h}_s^{\mathrm{H}} \boldsymbol{w}\right|^2}{\sigma_s^2}, \tag{3}$$

$$\gamma_{e,k} = \frac{\left|\boldsymbol{h}_{e,k}^{\mathrm{H}} \boldsymbol{w}\right|^2}{\sigma_{e,k}^2}, \forall k. \tag{4}$$

According to [26], the ASR of the SU can be described as

$$R = \left[\log_2(1+\gamma_s) - \max_{k \in \{1,\cdots,K\}} \log_2(1+\gamma_{e,k})\right]^+ \tag{5}$$

where $[x]^+ = \max\{x, 0\}$. The equation implies that the secure communication is realized when $R > 0$, and the greater R, the better secrecy performance is achieved [27].

As shown in Fig. 2, we assume that UAV employs UPA of dimension $N_u = N_1 \times N_2$ to achieve a high gain with a compact size, and the UAV downlink channel consists of a predominant LoS component and multiple single-bounce non-LoS (NLoS) components due to the highly directional and quasi-optical properties of the radio wave propagation [28].

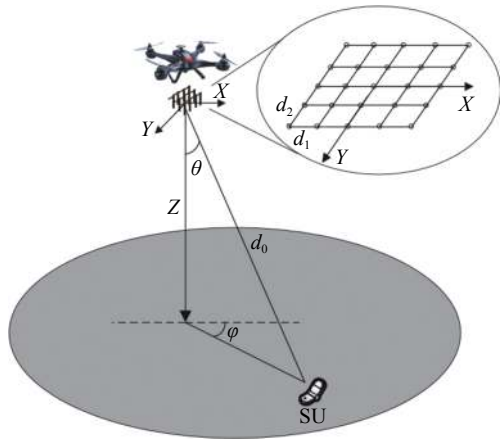

Fig. 2 Geometric relation between UAV and any user

Taking the effect of path loss into account, we obtain the UAV downlink channel vector $\boldsymbol{h}$ as

$$\boldsymbol{h} = \sqrt{g_e(\theta_0,\varphi_0)}\rho_0 \boldsymbol{a}_x(\theta_0,\varphi_0) \otimes \boldsymbol{a}_y(\theta_0,\varphi_0) + \sqrt{\frac{1}{L_n}} \sum_{m=1}^{L_n} \sqrt{g_e(\theta_m,\varphi_m)}\rho_m \boldsymbol{a}_x(\theta_m,\varphi_l) \otimes \boldsymbol{a}_y(\theta_m,\varphi_m) \tag{6}$$

where $\otimes$ denotes the Kronecker product, and L_n denotes the number of NLoS paths. ρ_0 and $\rho_m (m = 1, \cdots, L_n)$ are the pass loss associated with the LoS path and the mth NLoS path, respectively. The pass loss amplitude of the LoS component can be calculated as

$$|\rho_0|^2 = \left(\frac{\lambda}{4\pi d_0}\right)^2 \tag{7}$$

where λ is the wavelength and d_0 is the transmission distance. It should be pointed out that the value of $|\rho_m|^2$ is typically 5 dB to 10 dB lower than $|\rho_0|^2$ [29]. In addition, $g_e(\theta,\varphi)$ in (6) denotes the element pattern with θ and φ being the horizontal and vertical degree of arrival (DoA), respectively. According to the model introduced by International Telecommunication Union (ITU), $\hat{g}_e(\theta,\varphi) = 10\log_{10}(g_e(\theta,\varphi))$ with the element pattern in dB [30] can be expressed as

$$\hat{g}_e(\theta,\varphi)=E_{\max}-\min\{g_x(\theta,\varphi)+g_y(\theta,\varphi),S\} \tag{8}$$

where $E_{\max}$ represents the maximum antenna gain, S represents the side-lobe level, and $g_x(\theta,\varphi)$ and $g_y(\theta,\varphi)$ denote the relative patterns in X and Y planes, which can be, respectively, expressed as

$$g_x(\theta,\varphi)=\min\left\{12\left(\frac{\arctan(\cot\theta/\cos\varphi)}{\varphi_x^{3\text{dB}}}\right)^2,S\right\}, \tag{9}$$

$$g_y(\theta,\varphi)=\min\left\{12\left(\frac{\arctan(\tan\theta\sin\varphi)}{\varphi_y^{3\text{dB}}}\right)^2,S\right\}, \tag{10}$$

where $\varphi_x^{3\text{dB}}$ and $\varphi_y^{3\text{dB}}$ denote the 3 dB beamwidth of X and Y patterns, respectively. In (6), $\boldsymbol{a}_x(\theta,\varphi)$ and $\boldsymbol{a}_y(\theta,\varphi)$ are X and Y steering vectors of the UPA [31] and can be, respectively, expressed as

$$\boldsymbol{a}_x(\theta,\varphi)=\left[\mathrm{e}^{-\mathrm{j}\beta((N_1-1)/2)d_1\sin\theta\cos\varphi},\cdots,\mathrm{e}^{+\mathrm{j}\beta((N_1-1)/2)d_1\sin\theta\cos\varphi}\right]^{\mathrm{T}}, \tag{11}$$

$$\boldsymbol{a}_y(\theta,\varphi)=\left[\mathrm{e}^{-\mathrm{j}\beta((N_2-1)/2)d_2\sin\theta\sin\varphi},\cdots,\mathrm{e}^{+\mathrm{j}\beta((N_2-1)/2)d_2\sin\theta\sin\varphi}\right]^{\mathrm{T}}, \tag{12}$$

where $\beta=\dfrac{2\pi}{\lambda}$ denotes the wave number, and N_1 and N_2 are the number of array elements placed along X and Y axes, respectively. d_1 and d_2 are the inter-element spacing along X and Y axes, respectively.

Moreover, due to spectral sharing between the satellite and the UAV, the interference from UAV to PUs is also an important factor to be considered in the system design. The interference-to-noise ratio (INR) at the lth PU can be expressed as

$$\gamma_{p,l}=\frac{\left|\boldsymbol{h}_{p,l}^{\mathrm{H}}\boldsymbol{w}\right|^2}{\sigma_{p,l}^2},\quad l=1,\cdots,L \tag{13}$$

where $\boldsymbol{h}_{p,l}$ denotes the channel vector between the UAV and the lth PU, and $\sigma_{p,l}^2$ is the AWGN variance at the lth PU.

In addition, we assume the imperfect CSI of PUs and Eves is unknown, but the imperfect CSI based on angular information is available at the UAV, which can be expressed as

$$\boldsymbol{\Delta}_i=\{\theta_i\in[\theta_{i,Lo},\theta_{i,Up}],\varphi_i\in[\varphi_{i,Lo},\varphi_{i,Up}]\},\quad i\in\{(p,l),(e,k)\}. \tag{14}$$

In the considered CSUN, transmit power minimization and ASR maximization are both significant design criteria. In the following, we will first investigate the single objective problem under these two criteria separately. Then, we propose a trade-off design to balance two objectives through MOOP. By using (14), we formulate the worst-case ASR maximization problem subject to the quality-of-service (QoS) requirements of SU, the INR threshold of each PU and the total transmit power budget. The first problem can be expressed as

$P1$ (worst-case ASR maximization):

$$\begin{aligned}&\max_{\boldsymbol{w}}\min_{\boldsymbol{\Delta}_{e,k}}\ R\\ &\text{s.t.}\ \min_{\boldsymbol{\Delta}_{e,k}}R\geqslant R^{\min},\ \forall k,\\ &\max_{\boldsymbol{\Delta}_{p,l}}\gamma_{p,l}\leqslant\gamma^{\text{th}},\ \forall l,\\ &\boldsymbol{w}^{\mathrm{H}}\boldsymbol{w}\leqslant P^{\max},\end{aligned} \tag{15}$$

where $R^{\min}$ denotes the ASR threshold of SU, γ^{th} is the INR threshold of each PU and $P^{\max}$ represents the total transmit power budget.

Similarly, the second problem is designed to minimize the total transmit power, which can be expressed as

$P2$ (total transmit power minimization):

$$\begin{aligned}&\min_{\boldsymbol{w}}\boldsymbol{w}^{\mathrm{H}}\boldsymbol{w}\\ &\text{s.t.}\ \min_{\boldsymbol{\Delta}_{e,k}}R\geqslant R^{\min},\ \forall k,\\ &\max_{\boldsymbol{\Delta}_{p,l}}\gamma_{p,l}\leqslant\gamma^{\text{th}},\ \forall l,\\ &\boldsymbol{w}^{\mathrm{H}}\boldsymbol{w}\leqslant P^{\max}.\end{aligned} \tag{16}$$

Since a high achievable ASR leads to a high transmit power consumption and vice versa, the objectives of $P1$ and $P2$ are in conflict [31,32]. In order to obtain the Pareto optimal solution between these two single-objectives, we adopt the weighted Tchebycheff approach in [33] to formulate the MOOP as

$P3$ (multi-objective optimization):

$$\begin{aligned}&\min_{\boldsymbol{w}}\max_{j=1,2}\max_{\boldsymbol{\Delta}_{e,k}}\left\{\lambda_j\left(F_j(\boldsymbol{w})-F_j^*(\boldsymbol{w})\right)\right\}\\ &\text{s.t.}\ \min_{\boldsymbol{\Delta}_{e,k}}R\geqslant R^{\min},\ \forall k,\\ &\max_{\boldsymbol{\Delta}_{p,l}}\gamma_{p,l}\leqslant\gamma^{\text{th}},\ \forall l,\\ &\boldsymbol{w}^{\mathrm{H}}\boldsymbol{w}\leqslant P^{\max},\end{aligned} \tag{17}$$

where $F_1(\boldsymbol{w})=-\left\{\log_2(1+\gamma_s)-\max\limits_{k\in\{1,\cdots,K\}}\{\log_2(1+\gamma_{e,k})\}\right\}$ and $F_2(\boldsymbol{w})=\boldsymbol{w}^{\mathrm{H}}\boldsymbol{w}$. $F_j^*(\boldsymbol{w})$ is the optimal objective value of the jth problem and considered as a constant for $P3$. In addition, λ_j satisfying $\sum\lambda_j=1$ denotes a positive weighted variable that reflects the priority level of the jth objective from a systematic perspective and set by the decision-maker [34]. By varying the values of parameters λ_j, we can get a Pareto optimal set corresponding to a set of preference strategies for ASR and transmit power consumption. In particular, $P3$ is equivalent with Pj, when

$\lambda_j = 1$ and $\lambda_i = 0\ (i \neq j)$.

In the following, we will propose a robust BF scheme to solve the MOOP in (17).

3. Proposed multi-objective optimization based robust BF scheme

It can be observed that due to the continuity of CSI uncertainty sets, the constraints involve infinite inequality constraints that make problems difficult to be solved effectively. In order to overcome this predicament, we recast $P1$, $P2$ and $P3$ by introducing several auxiliary variables. Then, a method combining angular discretization with Taylor approximation is proposed to transform the intractable constraints into solvable forms. Finally, the MOOP can be solved efficiently.

First of all, by substituting (3)−(5) into (15), $P1$ can be derived as

$$\begin{aligned}
&\min_{\boldsymbol{w}} \max_{k\in\{1,\cdots,K\}} \max_{\boldsymbol{\Delta}_{e,k}} \\
&\left\{\log_2\left(1+\frac{\left|\boldsymbol{h}_{e,k}^{\mathrm{H}}\boldsymbol{w}\right|^2}{\sigma_{e,k}^2}\right)-\log_2\left(1+\frac{\left|\boldsymbol{h}_{s}^{\mathrm{H}}\boldsymbol{w}\right|^2}{\sigma_{s}^2}\right)\right\} \\
&\text{s.t.}\ \min_{\boldsymbol{\Delta}_{e,k}} \log_2\left(1+\frac{\left|\boldsymbol{h}_{s}^{\mathrm{H}}\boldsymbol{w}\right|^2}{\sigma_{s}^2}\right)- \\
&\log_2\left(1+\frac{\left|\boldsymbol{h}_{e,k}^{\mathrm{H}}\boldsymbol{w}\right|^2}{\sigma_{e,k}^2}\right)\geqslant R^{\min},\ \forall k, \\
&\max_{\boldsymbol{\Delta}_{p,l}} \frac{\boldsymbol{w}^{\mathrm{H}}\boldsymbol{h}_{p,l}\boldsymbol{h}_{p,l}^{\mathrm{H}}\boldsymbol{w}}{\sigma_p^2}\leqslant \gamma^{\mathrm{th}},\ \forall l, \\
&\boldsymbol{w}^{\mathrm{H}}\boldsymbol{w}\leqslant P^{\max}.
\end{aligned} \tag{18}$$

Denoting $\boldsymbol{W}=\boldsymbol{w}^{\mathrm{H}}\boldsymbol{w}$, $\boldsymbol{H}_s=\boldsymbol{h}_s\boldsymbol{h}_s^{\mathrm{H}}$, $\boldsymbol{H}_{e,k}=\boldsymbol{h}_{e,k}\boldsymbol{h}_{e,k}^{\mathrm{H}}$ and $\boldsymbol{H}_{p,l}=\boldsymbol{h}_{p,l}\boldsymbol{h}_{p,l}^{\mathrm{H}}$, the problem (18) can be further constructed as

$$\begin{aligned}
&\min_{\boldsymbol{W}\succcurlyeq 0} \max_{k\in\{1,\cdots,K\}} \max_{\boldsymbol{\Delta}_{e,k}} \left\{\log_2\left(\frac{\mathrm{Tr}(\boldsymbol{H}_{e,k}\boldsymbol{W})+\sigma_{e,k}^2}{\sigma_{e,k}^2}\right)-\right. \\
&\left.\log_2\left(\frac{\mathrm{Tr}(\boldsymbol{H}_{s}\boldsymbol{W})+\sigma_{s}^2}{\sigma_{s}^2}\right)\right\} \\
&\text{s.t.}\ \min_{\boldsymbol{\Delta}_{e,k}} \log_2\left(\frac{\mathrm{Tr}(\boldsymbol{H}_{s}\boldsymbol{W})+\sigma_{s}^2}{\sigma_{s}^2}\right)- \\
&\log_2\left(\frac{\mathrm{Tr}(\boldsymbol{H}_{e,k}\boldsymbol{W})+\sigma_{e,k}^2}{\sigma_{e,k}^2}\right)\geqslant R^{\min},\ \forall k, \\
&\max_{\boldsymbol{\Delta}_{p,l}} \frac{\mathrm{Tr}(\boldsymbol{H}_{p,l}\boldsymbol{W})}{\sigma_p^2}\leqslant \gamma^{\mathrm{th}},\ \forall l, \\
&\mathrm{Tr}(\boldsymbol{W})\leqslant P^{\max}, \\
&\mathrm{rank}(\boldsymbol{W})=1,
\end{aligned} \tag{19}$$

where $\mathrm{Tr}(\cdot)$ is the trace and $\mathrm{rank}(\cdot)$ represents the rank of a matrix. Since the objective function of (19) is nonconvex, we introduce slack variable to replace the objective function, and remove the nonconvex rank-one constraint which can be solved effectively by randomization technology [35]. Finally, the problem (19) can be converted into

$$\begin{aligned}
&\min_{\boldsymbol{W}\succcurlyeq 0,t} -t \\
&\text{s.t.}\ \min_{\boldsymbol{\Delta}_{e,k}} \log_2\left(\frac{\mathrm{Tr}(\boldsymbol{H}_{s}\boldsymbol{W})+\sigma_{s}^2}{\sigma_{s}^2}\right)- \\
&\log_2\left(\frac{\mathrm{Tr}(\boldsymbol{H}_{e,k}\boldsymbol{W})+\sigma_{e,k}^2}{\sigma_{e,k}^2}\right)\geqslant t,\ \forall k, \\
&\min_{\boldsymbol{\Delta}_{e,k}} \log_2\left(\frac{\mathrm{Tr}(\boldsymbol{H}_{s}\boldsymbol{W})+\sigma_{s}^2}{\sigma_{s}^2}\right)- \\
&\log_2\left(\frac{\mathrm{Tr}(\boldsymbol{H}_{e,k}\boldsymbol{W})+\sigma_{e,k}^2}{\sigma_{e,k}^2}\right)\geqslant R^{\min},\ \forall k, \\
&\max_{\boldsymbol{\Delta}_{p,l}} \frac{\mathrm{Tr}(\boldsymbol{H}_{p,l}\boldsymbol{W})}{\sigma_p^2}\leqslant \gamma^{\mathrm{th}},\ \forall l, \\
&\mathrm{Tr}(\boldsymbol{W})\leqslant P^{\max},
\end{aligned} \tag{20}$$

where t is an auxiliary variable. In order to address the non-convexity of constraints in (20), we introduce a set of auxiliary variables $\{x, y_k\}$, $\forall k$ and define the following equations:

$$e^x = \mathrm{Tr}(\boldsymbol{H}_s\boldsymbol{W})+\sigma_s^2, \tag{21}$$

$$e^{y_k} = \mathrm{Tr}(\boldsymbol{H}_{e,k}\boldsymbol{W})+\sigma_{e,k}^2,\ \forall k. \tag{22}$$

Substituting (21) and (22) into problem (20), we obtain

$$\begin{aligned}
&\min_{\boldsymbol{W}\succcurlyeq 0,t,x,y_k} -t \\
&\text{s.t. C1: } x\log_2 e-\log_2\sigma_s^2- \\
&y_k\log_2 e+\log_2\sigma_{e,k}^2\geqslant t,\ \forall k, \\
&\text{C2: } x\log_2 e-\log_2\sigma_s^2- \\
&y_k\log_2 e+\log_2\sigma_{e,k}^2\geqslant R^{\min},\ \forall k, \\
&\text{C3: } \mathrm{Tr}(\boldsymbol{H}_s\boldsymbol{W})+\sigma_s^2\geqslant e^x, \\
&\text{C4: } \max_{\boldsymbol{\Delta}_{e,k}} \mathrm{Tr}(\boldsymbol{H}_{e,k}\boldsymbol{W})+\sigma_{e,k}^2\leqslant e^{y_k},\ \forall k, \\
&\text{C5: } \max_{\boldsymbol{\Delta}_{p,l}} \mathrm{Tr}(\boldsymbol{H}_{p,l}\boldsymbol{W})\leqslant \gamma^{\mathrm{th}},\ \forall l, \\
&\text{C6: } \mathrm{Tr}(\boldsymbol{W})\leqslant P^{\max}, \\
&\text{C7: } t\geqslant 0.
\end{aligned} \tag{23}$$

It can be found that both the constraints C4 and C5 are mathematically intractable due to the channel uncertainty region $\boldsymbol{\Delta}_i$. Therefore, we adopt a method combining angular discretization with Taylor approximation to address the channel uncertain region in (23).

Let first discuss the uncertainty region $\boldsymbol{\Delta}_{e,k}$. According to the concept of convex hull, any CSI in the uncertainty region $\boldsymbol{\Delta}_{e,k}$ can be effectively expressed as a convex combination of a finite number of CSI sampling points. Thus,

we uniformly select M_1 and M_2 samples from vertical DoA set $\left[\theta_{e,k}^L, \theta_{e,k}^U\right]$ and horizontal DoA set $\left[\varphi_{e,k}^L, \varphi_{e,k}^U\right]$ as

$$\theta_{e,k}^{(i_1)} = \theta_{e,k}^L + (i_1 - 1)\Delta\theta_{e,k},\ \ i_1 = 1, \cdots, M_1, \tag{24}$$

$$\varphi_{e,k}^{(i_2)} = \varphi_{e,k}^L + (i_2 - 1)\Delta\varphi_{e,k},\ \ i_2 = 1, \cdots, M_2, \tag{25}$$

where $\Delta\theta_{e,k} = \left(\theta_{e,k}^U - \theta_{e,k}^L\right)/(M_1 - 1)$, and $\Delta\varphi_{e,k} = \left(\varphi_{e,k}^U - \varphi_{e,k}^L\right)/(M_2 - 1)$. $M_1 \geqslant N_1$ and $M_2 \geqslant N_2$ represent the number of samples on $\theta_{e,k}$ and $\varphi_{e,k}$, respectively. Besides, $\theta_{e,k}^{(i_1)}$ and $\varphi_{e,k}^{(i_2)}$ are the angular information of $\boldsymbol{h}_{e,k}^{(i_1,i_2)}$, respectively. Define the following equation:

$$\begin{aligned} &\boldsymbol{H}_{e,k}^{(j)} = \boldsymbol{h}_{e,k}^{(j)}\boldsymbol{h}_{e,k}^{(j)\mathrm{H}} = \boldsymbol{h}_{e,k}^{(i_1,i_2)}\boldsymbol{h}_{e,k}^{(i_1,i_2)\mathrm{H}}, \\ &j = 1, \cdots, (i_1 - 1)M_1 + i_2, \cdots, M_1M_2. \end{aligned} \tag{26}$$

According to (26), the convex hull $\boldsymbol{\Omega}_{e,k}$ of $\boldsymbol{\Delta}_{e,k}$ can be expressed as

$$\begin{aligned} \boldsymbol{\Omega}_{e,k} = \mathrm{conv}\left(\boldsymbol{\Delta}_{e,k}\right) = \Bigg\{ &\sum_{j=1}^{M_1M_2} \mu_{e,k}^j \boldsymbol{H}_{e,k}^{(j)} \Bigg| \\ &\boldsymbol{H}_{e,k}^{(j)} \in \boldsymbol{\Delta}_{e,k}, \mu_{e,k}^j \geqslant 0, \sum_{j=1}^{M_1M_2} \mu_{e,k}^j = 1 \Bigg\} \end{aligned} \tag{27}$$

where $\mu_{e,k}^j > 0$ is the weight of the j th discrete channel matrix $\boldsymbol{H}_{e,k}^{(j)}$. Thus, the constraint C4 can be conformed as

$$\max_{\boldsymbol{H}_{e,k} \in \boldsymbol{\Omega}_{e,k}} \mathrm{Tr}(\boldsymbol{H}_{e,k}\boldsymbol{W}) + \sigma_{e,k}^2 \leqslant e^{y_k},\ \ \forall k, \tag{28}$$

which is equivalent to

$$\max_{\left\{\mu_{e,k}^j\right\}} \sum_{j=1}^{M_1M_2} \mathrm{Tr}\left(\mu_{e,k}^j \boldsymbol{H}_{e,k}^{(j)}\boldsymbol{W}\right) + \sigma_{e,k}^2 \leqslant e^{y_k},\ \ \forall k. \tag{29}$$

In order to achieve the maximum value on the left side of (29), we adopt Cauchy-Schwarz inequality to calculate the weighting factor $\left\{\mu_{e,k}^j\right\}$. Specifically, we have

$$\begin{aligned} &\left(\sum_{j=1}^{M_1M_2} \mathrm{Tr}\left(\mu_{e,k}^j \boldsymbol{H}_{e,k}^{(j)}\boldsymbol{W}\right)\right)^2 \leqslant \\ &\left(\sum_{j=1}^{M_1M_2} \left(\mu_{e,k}^j\right)^2\right)\left(\sum_{j=1}^{M_1M_2} \left(\mathrm{Tr}\left(\boldsymbol{H}_{e,k}^{(j)}\boldsymbol{W}\right)\right)^2\right) \end{aligned} \tag{30}$$

where the equality is satisfied when

$$\frac{\mu_{e,k}^1}{\mathrm{Tr}\left(\boldsymbol{H}_{e,k}^{(1)}\boldsymbol{W}\right)} = \frac{\mu_{e,k}^2}{\mathrm{Tr}\left(\boldsymbol{H}_{e,k}^{(2)}\boldsymbol{W}\right)} = \cdots = \frac{\mu_{e,k}^{M_1M_2}}{\mathrm{Tr}\left(\boldsymbol{H}_{e,k}^{(M_1M_2)}\boldsymbol{W}\right)}. \tag{31}$$

Combining $\sum_{j=1}^{M_1M_2} \mu_{e,k}^j = 1$ and defining $\bar{\mu}_{e,k}^j$ as the optimal weight, we can obtain

$$\bar{\mu}_{e,k}^j = \frac{\mathrm{Tr}\left(\boldsymbol{H}_{e,k}^{(j)}\boldsymbol{W}\right)}{\sum_{j=1}^{M_1M_2} \mathrm{Tr}\left(\boldsymbol{H}_{e,k}^{(j)}\boldsymbol{W}\right)}. \tag{32}$$

Substituting (32) into (29) and defining $\bar{\boldsymbol{H}}_{e,k} = \sum_{j=1}^{M_1M_2} \bar{\mu}_{e,k}^j \boldsymbol{H}_{e,k}^{(j)}$, we obtain

$$\mathrm{Tr}\left(\bar{\boldsymbol{H}}_{e,k}\boldsymbol{W}\right) + \sigma_{e,k}^2 \leqslant e^{y_k}. \tag{33}$$

Note that the constraint (33) is still non-convex due to the exponential function, we adopt first-order Taylor expansion and obtain

$$\mathrm{Tr}\left(\bar{\boldsymbol{H}}_{e,k}\boldsymbol{W}\right) + \sigma_{e,k}^2 \leqslant e^{\bar{y}_k}(y - \bar{y}_k + 1) \tag{34}$$

where $\bar{y}_k$ is an initial feasible point and is defined as

$$\bar{y}_k = \ln\left(\mathrm{Tr}(\bar{\boldsymbol{H}}_{e,k}\boldsymbol{W}) + \sigma_{e,k}^2\right). \tag{35}$$

Similarly, constraint C5 can be reconstructed as

$$\mathrm{Tr}\left(\bar{\boldsymbol{H}}_{p,l}\boldsymbol{W}\right) \leqslant \gamma^{\mathrm{th}} \tag{36}$$

where

$$\bar{\boldsymbol{H}}_{p,l} = \sum_{j=1}^{M_1M_2} \bar{\mu}_{p,l}^j \boldsymbol{H}_{p,l}^{(j)}, \tag{37}$$

$$\bar{\mu}_{p,l}^j = \frac{\mathrm{Tr}\left(\boldsymbol{H}_{p,l}^{(j)}\boldsymbol{W}\right)}{\sum_{j=1}^{M_1M_2} \mathrm{Tr}\left(\boldsymbol{H}_{p,l}^{(j)}\boldsymbol{W}\right)}. \tag{38}$$

Substituting (34) and (36) into optimization problem (23), we obtain

$$\begin{aligned} &\min_{\boldsymbol{W} \succcurlyeq 0, t, x, y_k} \ -t \\ &\text{s.t. } \tilde{\mathrm{C}}1: x\log_2 e - \log_2\sigma_s^2 - \\ &y_k\log_2 e + \log_2\sigma_{e,k}^2 \geqslant t,\ \ \forall k, \\ &\tilde{\mathrm{C}}2: x\log_2 e - \log_2\sigma_s^2 - \\ &y_k\log_2 e + \log_2\sigma_{e,k}^2 \geqslant R^{\min},\ \ \forall k, \\ &\tilde{\mathrm{C}}3:\ \mathrm{Tr}(\boldsymbol{H}_s\boldsymbol{W}) + \sigma_s^2 \geqslant e^x, \\ &\tilde{\mathrm{C}}4:\ \mathrm{Tr}\left(\bar{\boldsymbol{H}}_{e,k}\boldsymbol{W}\right) + \sigma_{e,k}^2 \leqslant \\ &e^{\bar{y}_k}(y - \bar{y}_k + 1),\ \ \forall k, \\ &\tilde{\mathrm{C}}5:\ \mathrm{Tr}\left(\bar{\boldsymbol{H}}_{p,l}\boldsymbol{W}\right) \leqslant \gamma^{th},\ \ \forall l, \\ &\tilde{\mathrm{C}}6:\ \mathrm{Tr}(\boldsymbol{W}) \leqslant P^{\max}, \\ &\tilde{\mathrm{C}}7: t \geqslant 0. \end{aligned} \tag{39}$$

Similarly, $P2$ and $P3$ can be, respectively, transformed as

(i) Transformed P 2 (total transmit power minimization):

$$\min_{\boldsymbol{W}\succcurlyeq 0,t,x,y_k} \operatorname{Tr}(\boldsymbol{W})$$
$$\text{s.t. } \tilde{\mathrm{C}}_1-\tilde{\mathrm{C}}_7. \tag{40}$$

(ii) Transformed $P3$ (multi-objective optimization):

$$\min_{\boldsymbol{W}\succcurlyeq 0,t,x,y_k,\tau} \tau$$
$$\text{s.t. } \tilde{\mathrm{C}}_1-\tilde{\mathrm{C}}_7,$$
$$\lambda_j\left(F_j(\boldsymbol{w})-F_j^*(\boldsymbol{w})\right)\leqslant\tau, \tag{41}$$

where τ is the introduced slack variable. It can be observed that the final problem (41) is convex and can be efficiently solved by CVX.

Finally, the proposed BF algorithm is shown in Algorithm 1. The complexity is $O\left(\sqrt{3K+L+5}\cdot n\cdot[(3K+L+5)(1+n)+n^2]\right)$ where $n=O(N_u^2+3+K)$ [36].

Algorithm 1 The proposed multi-objective optimization based robust BF algorithm

Input: $\left\{\boldsymbol{h}_s,\boldsymbol{\Delta}_{e,k},\boldsymbol{\Delta}_{p,l},\sigma_s^2,\sigma_{e,k}^2,\sigma_{p,l}^2\right\}$ and $R^{\min}$, γ^{th}, $P^{\max}$.

1. Set the tolerance of accuracy ε, the maximum number of iteration $N_{\max}$, the discrete number M_1 and M_2;
2. Set the initial discrete channel weight $\left(\mu_{e,k}^j\right)^{(0)}$ and $\left(\mu_{p,l}^j\right)^{(0)}$;
3. Initialize the algorithm with feasible solution $\{\boldsymbol{w}^{(0)}\}$ and $\left\{\boldsymbol{W}^{(0)}=\boldsymbol{w}^{(0)}(\boldsymbol{w}^{(0)})^{\mathrm{H}}\right\}$;
4. Set the iteration number $n=0$;
5. **repeat**
6. Obtain $(\bar{y}_k)^{(n+1)}$ through (35);
7. Solve the MOOP (41) to obtain the optimal solution $\boldsymbol{W}^{(n+1)*}$;
8. Update $(\mu_{e,k}^j)^{(n+1)}$ and $(\mu_{p,l}^j)^{(n+1)}$ through (32) and (38);
9. Calculate $\eta=\left\|\boldsymbol{W}^{(n+1)*}-\boldsymbol{W}^{(n)*}\right\|$;
10. $n=n+1$;
11. **Until** $\eta\leqslant\varepsilon$ or $n=N_{\max}$;
12. Use the randomization technology to achieve an optimal solution $\boldsymbol{w}^*$.

Output: Optimal BF vector $\boldsymbol{w}^*$.

4. Numerical results and discussion

In this section, computer simulations are conducted to evaluate the performance of the proposed robust BF scheme for a CSUN in the presence of L=2 and K=2. All of the plots are obtained by performing 10 000 channel realizations. We set the tolerance of accuracy ε=10^{-3}, the maximum number of iteration $N_{\max}$ = 10. Other parameters are listed in Table 1 [6]. Moreover, we compare the proposed robust BF scheme with three different BF schemes, namely, zero forcing (ZF) BF scheme, maximum ratio transmission (MRT) BF scheme and non-robust BF scheme.

Table 1 Main simulation parameters

Parameter	Value
UAV height/km	1
UPA	8×8
Carrier frequency/GHz	2
3 dB angle/(°)	$\varphi_x^{3\mathrm{dB}}=60$, $\varphi_y^{3\mathrm{dB}}=10$
Antenna inter-element spacing	$d_1=d_2=\lambda/2$
Side-lobe level/dB	$S_m=20$
Bandwidth/KHz	B=500
Noise temperature/K	T = 300

Fig. 3 and Fig. 4 plot the beampatterns of the BF weight vector obtained by the proposed robust BF scheme from 3D and vertical vision, respectively. It can be observed that the maximum direction of beam points to the SU, and four nulls are generated with at least −50 dB at the uncertainty region of PUs and Eves, respectively, demonstrating that our proposed robust BF scheme can effectively guarantee the signal quality at the intended user and suppress the signal leaked to unintended users among the uncertainty regions.

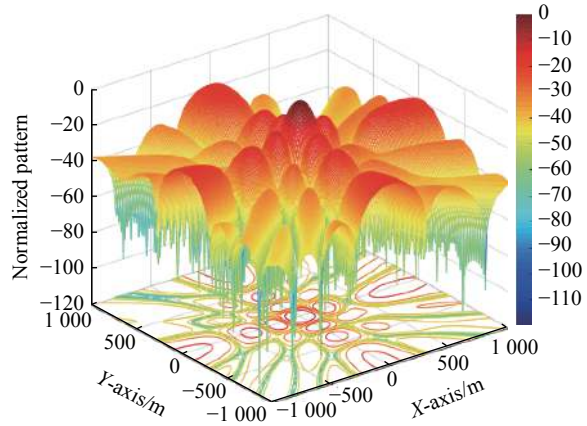

Fig. 3 3D beampattern of w

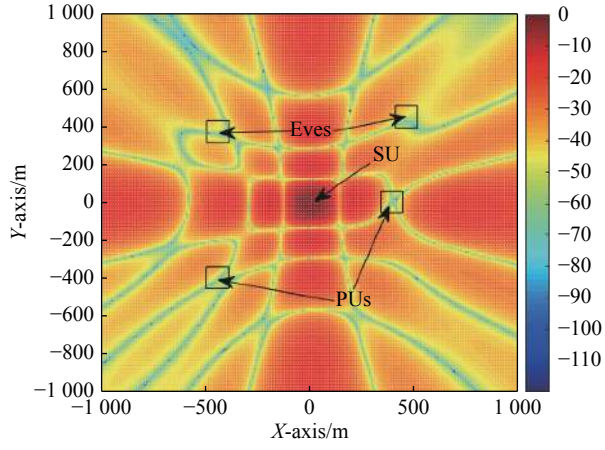

Fig. 4 Beampattern from vertical vision

Fig. 5 depicts trade-off regions for the ASR and total transmit power of the four schemes. The curve is obtained from $P3$ by varying the values of $\lambda_j \geqslant 0$ by the step of 0.1 subject to $\sum \lambda_j = 1$. It can be observed that the ASR of SU is a monotonically increasing function with respect to the total transmit power. It can be observed that the ASR of the nonrobust BF scheme, MRT BF scheme and ZF BF scheme would converge gradually as the transmit power grows. Moreover, our proposed robust BF scheme has the superior performance to the other three schemes and the difference becomes larger as the total transmit power increases. The reason is that the proposed robust BF scheme takes the channel uncertainty region into consideration, having good robustness, and can well deal with the performance loss caused by channel errors. The curves verify the superiority and security of our proposed robust BF scheme.

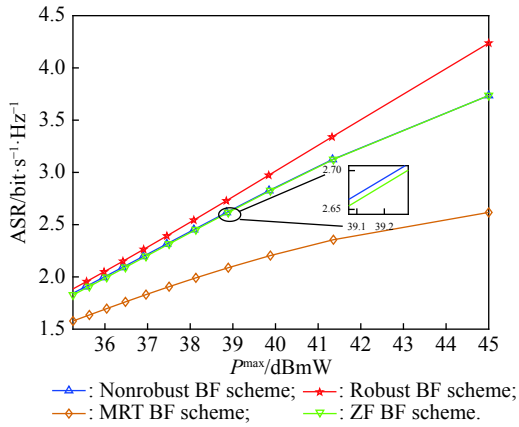

Fig. 5 ASR versus total transmit power

Fig. 6 plots the trade-off region for the INR and the total transmit power. It can be seen that the INR of our proposed scheme increases slowly with the total transmit power and is below the threshold $\gamma^{\text{th}} = -50$ dB. Moreover, other three schemes cannot satisfy the QoS requirement of PUs. As the increase of power, they will produce serious interference to PUs. Therefore, our proposed robust scheme outperforms the other schemes significantly.

Fig. 7 depicts the relationship between the total transmit power, INR and ASR. The weighted MOOP is set as λ_1=λ_2=0.5. It can be observed that the total transmit power increases as the ASR threshold increases because more total transmit power is needed to satisfy the increasing requirement of ASR. However, the INR threshold has a small influence on the total transmit power. The main reason is that our proposed robust BF scheme can effectively suppress the interference to the PU.

Fig. 8 illustrates the ASR against the antenna number of UAV. It can be observed that the difference between the proposed scheme and the other schemes becomes larger as the antenna number increases. The reason is that employing more antennas can enhance the advantage of the proposed scheme, but will both simultaneously increase the signal strength of SU and Eves in the other schemes, thus eventually increase the performance gap. The curves verify the superiority of our proposed robust BF scheme.

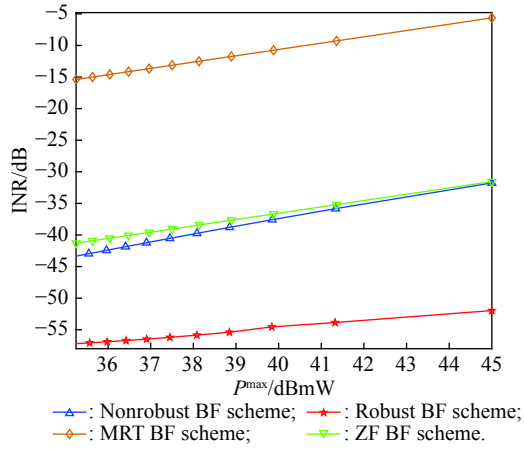

Fig. 6 INR versus total transmit power

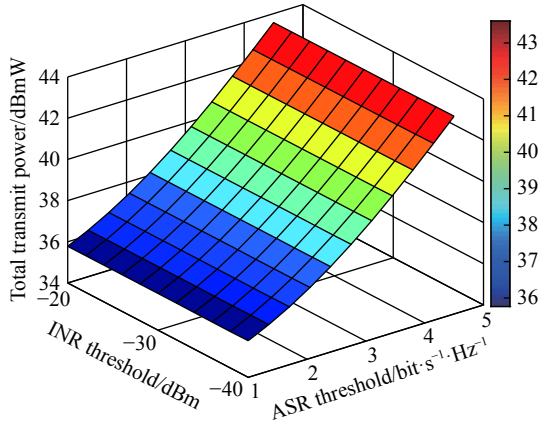

Fig. 7 Total transmit power versus INR and ASR

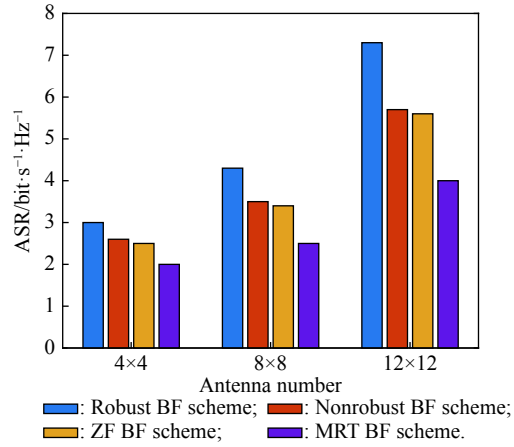

Fig. 8 ASR versus antenna number of UAV

5. Conclusions

By using the weighted Tchebycheff approach, we propose a multi-objective robust secure BF scheme in the CSUN to jointly considering the ASR and the total transmit power, where only imperfect CSI of PUs and Eves is available at the UAV. Specifically, we formulate a MOOP under the constraints of minimum ASR of SUs, QoS requirement of PUs and total transmit power budget. Then, we propose a method combining angular discretization with Taylor approximation to transform the MOOP into convex one. Next, we adopt SDP along with randomization technology to solve the MOOP and obtain the BF weight vector. Finally, Monte Carlo simulation results demonstrate the effectiveness and superiority of the proposed robust BF scheme.

References

[1] LIN M, HUANG Q Q, COLA T D, et al. Integrated 5G-satellite networks: a perspective on physical layer reliability and security. IEEE Wireless Communications, 2020, 27(6): 152–159.

[2] HUANG Q Q, LIN M, ZHU W P, et al. Performance analysis of integrated satellite-terrestrial multiantenna relay networks with multiuser scheduling. IEEE Trans. on Aerospace and Electronic Systems, 2020, 56(4): 2718–2731.

[3] SUN H Q, XIA W, HU X X, et al. Earth observation satellite scheduling for emergency tasks. Journal of Systems Engineering and Electronics, 2019, 30(5): 931–945.

[4] MENG S F, SHU J S, YANG Q, et al. Analysis of detection capabilities of LEO reconnaissance satellite constellation based on coverage performance. Journal of Systems Engineering and Electronics, 2018, 29(1): 98–104.

[5] MOZAFFARI M, SAAD W, BENNIS M, et al. A tutorial on UAVs for wireless networks: applications, challenges, and open problem. IEEE Communications Surveys and Tutorials, 2019, 21(3): 2334–2360.

[6] KONG H C, LIN M, ZHU W P, et al. Multiuser scheduling for asymmetric FSO/RF links in satellite-UAV-terrestrial networks. IEEE Wireless Communications Letters, 2020, 9(8): 1235–1239.

[7] LIN Z, LIN M, COLA T D, et al. Supporting IoT with rate-splitting multiple access in satellite and aerial integrated networks. IEEE Internet of Things Journal, 2021, 8(14): 11123–11134.

[8] XU Z, ZHANG E, CHEN Q W. Rotary unmanned aerial vehicles path planning in rough terrain based on multi-objective particle swarm optimization. Journal of Systems Engineering and Electronics, 2020, 31(1): 130–141.

[9] HUANG Q Q, LIN M, ZHU W P, et al. Uplink massive access in mixed RF/FSO satellite-aerial-terrestrial networks. IEEE Trans. on Communications, 2021, 69(4): 2413–2426.

[10] LI B, FEI Z S, ZHANG Y. UAV communications for 5G and beyond: recent advances and future trends. IEEE Internet of Things Journal, 2019, 6(2): 2241–2263.

[11] LIU C X, FENG W, CHEN Y F, et al. Cell-free satellite-UAV networks for 6G wide-area internet of things. IEEE Journal on Selected Areas in Communications, 2021, 39(4): 1116–1131.

[12] HUANG Q Q, LIN M, WANG J B, et al. Energy efficient beamforming schemes for satellite-aerial-terrestrial networks. IEEE Trans. on Communications, 2020, 68(6): 3863–3875.

[13] RUAN Y H, LI Y, ZHANG R, et al. Cooperative resource management for cognitive satellite-aerial-terrestrial integrated networks towards IoT. IEEE Access, 2020, 8: 35759–35769.

[14] KALANTARI A, ZHENG G, GAO Z, et al. Secrecy analysis on network coding in bidirectional multibeam satellite communications. IEEE Trans. on Information Forensics and Security, 2015, 10(9): 1862–1874.

[15] LIN Z, LIN M, OUYANG J, et al. Beamforming for secure wireless information and power transfer in terrestrial networks coexisting with satellite networks. IEEE Signal Processing Letters, 2018, 25(8): 1166–1170.

[16] LIN Z, LIN M, CHAMPAGNE B, et al. Secure and energy efficient transmission for RSMA-based cognitive satellite-terrestrial networks. IEEE Wireless Communication Letters, 2021, 10(2): 251–255.

[17] ARTI M K. Channel estimation and detection in hybrid satellite-terrestrial communication systems. IEEE Trans. on Vehicular Technology, 2016, 65(7): 5764–5771.

[18] LI B, FEI Z S, CHU Z, et al. Secure transmission for heterogeneous cellular networks with wireless information and power transfer. IEEE Systems Journal, 2018, 12(10): 3755–3766.

[19] YAN Y, YANG W W, GUO D X, et al. Robust secure beamforming and power splitting for millimeter-wave cognitive satellite –terrestrial networks with SWIPT. IEEE Systems Journal, 2020, 14(3): 3233–3244.

[20] NG D W K, XIANG L, SCHOBER R. Multi-objective beamforming for secure communication in systems with wireless information and power transfer. Proc. of the 24th Annual International Symposium on Personal, Indoor, and Mobile Radio Communications, 2013: 7−12.

[21] LI Z, GONG S Q, XING C W, et al. Multi-objective optimization for distributed MIMO networks. IEEE Trans. on Communications, 2017, 65(10): 4247–4259.

[22] SUN Y, NG D W K, ZHU J, et al. Multi-objective optimization for robust power efficient and secure full-duplex wireless communication systems. IEEE Trans. on Wireless Communications, 2016, 15(8): 5511–5526.

[23] YIN C Y, LIN Z, TAO X S, et al. Secure beamformer design for cognitive satellite terrestrial networks. Proc. of the IEEE 4th International Conference on Computer and Communications, 2018: 997−1002.

[24] MIETTINEN L. Nonlinear multiobjective optimization. Boston: Kluwer Academic Publishers, 1999.

[25] HOYHTYA M, KYROLAINEN J, HULKKONEN A, et al. Application of cognitive radio techniques to satellite communication. Proc. of the IEEE International Symposium on Dynamic Spectrum Access Networks, 2012: 540−551.

[26] CUMANAN K, DING Z G, XU M, et al. Secrecy rate optimization for secure multicast communications. IEEE Journal of Selected Topics in Signal Processing, 2016, 10(8): 1417–1432.

[27] CSISZAR I, KORNER J. Broadcast channels with confidential messages. IEEE Trans. on Information Theory, 1978, 24(3): 339–348.

[28] LIN M, LIN Z, ZHU W P, et al. Joint beamforming for secure communication in cognitive satellite terrestrial networks. IEEE Journal on Selected Areas in Communications, 2018, 36(5): 1017–1029.

[29] LIN Z, LIN M, WANG J B. Joint beamforming and power allocation for satellite-terrestrial integrated networks with

non-orthogonal multiple access. IEEE Journal of Selected Topics in Signal Processing, 2019, 13(3): 657–670.
[30] International Telecommunication Union. Guidelines for evaluation of radio interface technologies for IMT-advanced. Document ITU-R M. 2135. Geneva: International Telecommunication Union, 2008.
[31] ZHU H L, WANG J Z. Chunk-based resource allocation in OFDMA systems—part I: chunk allocation. IEEE Trans. on Communications, 2009, 57(9): 2734–2744.
[32] ZHU H L, WANG J Z. Chunk-based resource allocation in OFDMA systems—part II: joint chunk, power and bit allocation. IEEE Trans. on Communications, 2012, 60(2): 499–509.
[33] FEI Z S, LI B, YANG S S, et al. A survey of multi-objective optimization in wireless sensor networks: metrics, algorithms, and open problems. IEEE Communications Surveys & Tutorials, 2017, 19(1): 550–586.
[34] MARLER R, ARORA J. Survey of multi-objective optimization methods for engineering. Structural and Multidisciplinary Optimization, 2004, 26(6): 369–395.
[35] LUO Z Q, MA W K, SO M C, et al. Semidefinite relaxation of quadratic optimization problems. IEEE Signal Processing Magazine, 2010, 27(3): 20–34.
[36] LI B, FEI Z S, CHU Z, et al. Robust chance-constrained secure transmission for cognitive satellite-terrestrial networks. IEEE Trans. on Vehicular Technology, 2018, 67(5): 4208–4219.

Biographies

WANG Zining was born in 1997. He received his B.S. degree from Nanjing University of Posts and Telecommunications, Nanjing, China, in 2019. He is currently pursuing his Ph.D. degree in signal and information processing with Nanjing University of Posts and Telecommunications, Nanjing, China. His research interests include wireless communication and intelligent signal processing.
E-mail: wzn_email@163.com

LIN Min was born in 1972. He received his B.S. degree from National University of Defense Technology, Changsha, China, in 1993, M.S. degree from Nanjing Institute of Communication Engineering, Nanjing, China, in 2000, and Ph.D. degree from Southeast University, Nanjing, in 2008, all in electrical engineering. From Apr. 2015 to Oct. 2015, he visited University of California, Irvine, as a senior research fellow. He is currently a professor and supervisor of Ph.D. and graduate students with Nanjing University of Posts and Telecommunications, Nanjing, China. His research interests include wireless communications and array signal processing.
E-mail: linmin@njupt.edu.cn

TANG Xiaogang was born in 1977. He is currently an assistant professor of Xi'an Jiaotong University and Space Engineering University, Beijing, China. His research interests include mechatronics, pattern recognition, signal processing, and satellite communication.
E-mail: titantxg@163.com

GUO Kefeng was born in 1990. He is currently an assistant professor with the School of Space Information, Space Engineering University. His current research interests are cooperative relay networks, MIMO communications, satellite communication, cognitive radio, NOMA technology and physical layer security.
E-mail: guokefeng.cool@163.com

HUANG Shuo was born in 1985. He is now a senior engineer in Shanghai Aerospace Electronic Technology Institute. His current research interests include electronic engineering and satellite communications.
E-mail: hskidd@163.com

CHENG Ming was born in 1991. He received his B.S. degree in information engineering from Nanjing University of Aeronautics and Astronautics in 2012, M.S. degree in communications engineering from Nanjing University of Aeronautics and Astronautics in 2015, and Ph.D. degree from Southeast University in 2020. His current research interests include applications of stochastic geometry, millimeter wave communications, massive MIMO, and intelligent reflecting surface.
E-mail: mingcheng@njupt.edu.cn